Journal of Inorganic Biochemistry 181 (2018) 18–27

Contents lists available at ScienceDirect

Journal of Inorganic Biochemistry

journal homepage: www.elsevier.com/locate/jinorgbio

Ruthenium dendrimers as carriers for anticancer siRNA

Sylwia Michlewska[a,b], Maksim Ionov[b,*], Marta Maroto-Díaz[c,d], Aleksandra Szwed[b], Aliaksei Ihnatsyeu-Kachan[e], Svetlana Loznikova[e], Dzmitry Shcharbin[e], Marek Maly[f], Rafael Gomez Ramirez[c,d], Francisco Javier de la Mata[c,d], Maria Bryszewska[b]

[a] Laboratory of Microscopic Imaging and Specialized Biological Techniques, Faculty of Biology and Environmental Protection, University of Lodz, Banacha12/16, 90-237 Lodz, Poland
[b] Department of General Biophysics, University of Lodz, Pomorska 141/143, 90-236 Lodz, Poland
[c] Departamento Química Orgánica y Química Inorganica, Universidad de Alcala de Henares, Spain
[d] Networking Research Center on Bioengineering, Biomaterials and Nanomedicine (CIBER-BBN), Spain
[e] Institute of Biophysics and Cell Engineering of NASB, Akademicheskaja 27, Minsk 220072, Belarus
[f] Department of Physics, Faculty of Science, J. E. Purkinje University in Ústí nad Labem, Ústí nad Labem, Czech Republic

ARTICLE INFO

Keywords:
Dendrimer
Ruthenium
siRNA
Drug delivery
Computer modeling
Molecular dynamics

ABSTRACT

Dendrimers, which are considered as one of the most promising tools in the field of nanobiotechnology due to their structural organization, showed a great potential in gene therapy, drug delivery, medical imaging and as antimicrobial and antiviral agents. This article is devoted to study interactions between new carbosilane-based metallodendrimers containing ruthenium and anti-cancer small interfering RNA (siRNA). Formation of complexes between anti-cancer siRNAs and Ru-based carbosilane dendrimers was evaluated by transmission electron microscopy, circular dichroism and fluorescence. The zeta-potential and the size of dendriplexes were determined by dynamic light scattering. The internalization of dendriplexes were estimated using HL-60 cells. Results show that ruthenium dendrimers associated with anticancer siRNA have the ability to deliver siRNA as non-viral vectors into the cancer cells. Moreover, dendrimers can protect siRNA against nuclease degradation. Nevertheless, further research need to be performed to examine the therapeutic potential of ruthenium dendrimers as well as dendrimers complexed with siRNA and anticancer drugs towards cancer cells.

1. Introduction

In normal cells, regulation of apoptosis is controlled by the synthesis of anti-apoptotic B-cell lymphoma 2 (Bcl-2) proteins [1,2]. One of the characteristics of cancer cells is enhanced synthesis of these Bcl-2 family proteins [3]. Neoplastic cells lose the ability to regulate apoptosis. Transfection into cancer cells of siRNAs complementary to the anti-apoptotic proteins, Bcl-xL, Bcl-2, Bcl-W, Mcl-xl (myeloid cell leukemia protein) and Bcl-B, is possible. It can lead to inhibition of their synthesis by an interference process [1,2,4,5] The serious limitation of such treatment is the effective delivery of siRNAs to cancer cells [6]. Due to the negative charge of siRNAs, they cannot effectively cross the plasma membrane. An additional problem is the possible degradation of nucleic acid by endonucleases before the start of the interference process [3]. Using nanomaterials as transfection vehicles for siRNAs can significantly improve nucleic acid internalization into cancer cells. Such nanocarriers should be positively charged, monodispersed and non-toxic to normal cells. Among a wide range of polymeric drug carriers that can be used in nanomedicine, dendrimers are the most promising nanoparticles, due their size, surface charge and solubility in water. Some of dendrimers can be used in therapy of HIV, cancers and genetic diseases [7–10]. The possibility of using dendrimers in gene silencing has been intensively studied [11].

Complexes of siRNAs with dendrimers can protect them from degradation by RNases [12]. Moreover, such complexes are positively charged [13,14], which allows them to interact easily with negatively charged cell membranes and enter cells by endocytosis [14].

Dendrimers are synthesized in a controlled manner. They consist of a core and attached repetitive units (branches) in the form of successive layers that create increasingly higher generations [7,13,15]. There are functional groups at the ends of branches that can be connected to substituents. The presence of surface groups determines dendrimer properties, such as a shape, size and charge [13]. Dendrimers are monodispersive and stable [1]. Due to the large number of charged end groups, they can form complexes with nucleic acids [16–18]. They can enter cells without damaging them [5]. Different types of dendrimers

* Corresponding author at: Department of General Biophysics, University of Lodz, Pomorska st. 141/143, Lodz 90-236, Poland.
E-mail address: maksion@biol.uni.lodz.pl (M. Ionov).

https://doi.org/10.1016/j.jinorgbio.2018.01.001
Received 20 September 2017; Received in revised form 29 December 2017; Accepted 7 January 2018
Available online 12 January 2018
0162-0134/ © 2018 Elsevier Inc. All rights reserved.

can have quite different properties; for instance, cationic carbosilane dendrimers (CBS) have been used as non-viral carriers delivering human immunodeficiency virus (HIV)-peptides into dendritic cells [7], whereas amine-terminated poly-(amidoamine) PAMAM dendrimers were applied as a complex to deliver siRNAs to lung alveolar epithelial A549 cells, resulting in genes silencing [6] PAMAM dendrimers were applied to create complexes with siRNAs and deliver it to lung alveolar epithelial A549 cells, resulting in genes silencing. There is much evidence that nucleic acid form complexes with phosphorus, carbosilane, and PAMAM dendrimers, with increasing transfection efficiency of DNA and RNA into cells [5,19,20]. Current attempts to modify the dendrimers for greater efficiency have been undertaken; Hashemi et al. 2016 [15] indicated that heterocyclic amine-modified poly-(amidoamine) and poly-(propylenimine) dendrimers facilitate gene delivery to neuroblastoma cells. Other modifications involve the supply of anti-cancer drugs or metal ions, such as gold, silver, platinum and ruthenium that have anti-tumour properties.

Ruthenium metal can have different oxidation states. While Ru (III) complexes are considered as prodrug and are non-toxic to healthy tissues, Ru (II) derivatives are in general cytotoxic against cancer cells [21]. Like iron, ruthenium can form complexes with transferrin and albumin [22,23]. In the cancer cells, ruthenium will react with and damage DNA, leading to cell death [24]. To increase the anti-cancer properties of ruthenium, it can be combined with anti-cancer siRNAs, creating a new agent for treatment for a range of tumours. Here we have tried to characterize the biophysical properties of new ruthenium-terminated dendrimers [25] complexed with anti-cancer siRNAs. Ruthenium dendrimers form stable positively charged complexes with siBcl RNAs, protecting them from degradation by RNases.

2. Experimental section

2.1. Structures of siRNA

Three different siRNAs and one scrambled siRNA were synthesized (Darmacon, Inc). All siRNA were labelled with fluorescein for electrophoresis runs. The sequences of the siRNA are presented in the Supporting information.

2.2. Computer modeling of siRNA-dendrimer interactions

3D computer models of dendrimer structures were created using dendrimer builder, as implemented in the Materials Studio software package from BIOVIA (formerly Accelrys). GAFF force field (Generalized Amber Force Field), was used for parameterization of dendrimers [48] The RESP technique [49] was employed for calculation of dendrimer atoms partial charges. Charge parameterization was performed by using R.E.D.-IV tools [50]. QM calculations, necessary for partial charges derivation and calculation of missing force field parameters, were done using GAMESS software [51]. The pmemd.cuda module [52] from Amber16 [53] package was employed for Molecular Dynamics simulations. The initial configurations of the dendrimer/siRNA complexes were prepared using UCSF Chimera software which was also employed for final visualizations [54]. See Supporting information for more details.

2.3. Zeta potential measurements

A Laser Doppler Velocimetry technique by Zetasizer Nano ZS-90, Malvern Instruments (UK) was used to estimate zeta potential of dendrimer/siRNA complexes. The zeta potential value was calculated directly from the Helmholtz-Smoluchowski equation using Malvern software. The samples of dendriplexes were prepared at dendrimer/siRNA complexes at charge ratios from 0.5 to 10, the concentration of siRNA 0.3 μM, in 10 mM Na phosphate buffer, pH 7.4, at 22 °C. Seven to 10 measurements of zeta potential were collected for each sample and the results were averaged.

2.4. Hydrodynamic diameter measurement

Nanoparticle size was measured by dynamic light scattering (DLS) in a photon correlation spectrometer (Zetasizer Nano-ZS, Malvern Instruments, UK). The complexes at dendrimer/siRNA charge ratios from 0.5 to 10, the concentration of siRNA 0.3 μM were placed in plastic cells (DTS0012; Malvern) in 10 mM Na-phosphate buffer, pH 7.4, measurement being taken at the room temperature. The results were obtained in 5 independent replicates containing at least 3 scans of each one and shown as a mean ± SD. Data were analysed using Malvern Software.

2.5. Transmission electron microscopy (TEM)

Complexes of dendrimer and siRNA were prepared by mixing in 10 mM Na-phosphate buffer, pH 7.4. The charge ratio of the dendriplexes was (5–10):1 (dendrimer/siRNA) with the concentration of siRNA 3 μM. After a 10 min incubation at room temperature, 15 μl of each complex were placed on 200 mesh copper grid with carbon-coated surface for 10 min. The samples were stained with a saturated solution of uranyl acetate for 20 min. Images were taken with a JEOL-1010 (Japan) transmission electron microscope at 15–100,000× magnification to determine dendriplex morphology. Images have been sharpened to improve the contrast.

2.6. Ethidium bromide (EB) intercalation assay

To assess the interaction of dendrimers with siRNA, the ethidium bromide intercalation assay was used; as a fluorescent dye, it intercalates between the base pairs of nucleic acid. The dendrimers can interact with nucleic acids and displace EB from its intercalation sites, therefore fluorescence quenching occurs [26,4]. Fluorescence intensity was measured with the Perkin -Elmer LS-50B fluorescence spectrometer at 22 °C. Concentrations of 0.5 μM EB and 0.35 μM siRNA in 10 mM Na-phosphate buffer pH 7.4 were used for fluorescence experiments, where the wavelength of excitation was 480 nm and 650 nm for emission. Increasing concentrations of dendrimers were added to EB/siRNA solution at dendrimer/siRNA charge ratios ranging from 0.1 to 20. Fluorescence intensity values were recalculated as F/F_0, where F_0 is the fluorescence of EB intercalated into siRNA, and F the intensity EB fluorescence in presence of siRNA complexed with CRDs.

2.7. Circular dichroism and its analysis

Circular dichroism (CD) was measured with a J-815CD spectrometer (Jasco, Japan). Dendrimer/siRNA complexes were prepared in a 10 mM Na-phosphate buffer, pH 7.4, at charge ratios ranging from 0.5 to 20 with the concentration of siRNA, 2.5 μM. Samples at the final dendrimer/siRNA charge ratio were treated with 0.082 mg/ml heparin to release siRNA from the complex with dendrimers. The measurements were made between 200 and 300 nm with a 0.5 cm path-length in a Helma quartz cell. The scan parameters were as follows: 50 nm/min scan speed, 0.5 nm step resolution, 4 s response time, 1.0 nm bandwidth, with the slit was set to auto. CD spectra are given as the average of at least 3 independent scans. The mean ellipticity was calculated using software provided by Jasco.

2.8. Gel electrophoresis

Dendrimer/siRNA complexes were separated by agarose gel electrophoresis; they were mixed with negatively charged siRNA labelled with fluorescein. Samples were prepared in 10 mM Na-phosphate buffer, pH 7.4 with siRNA at 2 μM. To assess the protective effect of dendrimers from siRNA degradation, the dendriplexes were treated with RNase A (3.0 μg/ml) for 30 min at 37 °C. After 10 min incubation on ice, heparin at 0.082 mg/ml was added. Finally, the samples were placed on 3% agarose gel containing GelRed stain and separated by

electrophoresis in Tris-acetate-EDTA (TAE) buffer for 45 min at 90 V/35 mA. The bands on the gels were visualized with ultraviolet (UV) light.

2.9. Cellular uptake

To estimate the internalization of dendriplexes into HL-60 cells, fluorescein labelled siMcl-1 was used with flow cytometry and confocal microscopy. The cells were seeded at 1×10^5 cells per well on 24-well plates in RPMI medium contained 10% fetal bovine serum (FBS) and 1% antibiotic (peniciline/streptomicine) in humidified atmosphere containing 5% CO_2/95% air at the 37 °C. They were washed twice with phosphate-buffered saline (PBS) after a 3 h incubation with the dendrimer/siRNA complexes. The concentration of siRNA was 100 nM and the dendrimer/siRNA charge ratio 5:1. Measurements were made on a Becton Dickinson LSRII flow cytometer, with acquisition of 15,000 events in the [P6] gate at 488 nm excitation wavelength, whereas emission was recorded at 530 ± 30 nm wavelength. Data were analysed using FACSDiva software.

For confocal microscopy, the cells were stained with Dapi and Texas Red-X Phalloidin. Images were taken with a Leica TCS SP8 microscope at different wavelengths (405, 495 and 565 nm). Leica software was applied to analyse the data.

2.10. Statistical analysis

The results were statistically analysed with the t-test (in case of normal distribution) or the Mann-Whitney Rank Sum Test (where there was a lack of normal distribution). To assess the significance of differences between particular dendrimers, the ANOVA test was used. Where differences arose, further analysis used the Luke's method. Significance was set at $p < .05$.

3. Results

3.1. Ruthenium-terminated carbosilane dendrimers (CRD)

Two types of newly synthetized ruthenium terminated carbosilane dendrimers (imine-pyridine and pyridine end-groups) have been investigated. The main characteristics and synthesis of applied dendrimers have already been described [25,21]. The characteristics of dendrimers are given in Table 1 and Fig. 1.

3.2. Computer modeling

The ability of carbosilane ruthenium dendrimer CRD13 to interact with the siRNA (Bcl-xl) was analyzed by computer modeling. Molecular simulations confirmed, that dendrimer CRD13 is able to create stable complexes with siRNA (see Figs. 2 and 3 (main text) and Fig. 1 in Supporting information). Two dendrimer/siRNA systems were simulated. The first one (system **A** (Fig. 2)) was composed of 2 dendrimers and 1 siRNA (± charge ratio 0.2, length of simulation 150 ns), the second one (system **B** (Fig. 3)) contained 20 dendrimers and 1 siRNA (± charge ratio 2, length of simulation 70 ns).

Table 1
Number of surface groups and generations of ruthenium-terminated carbosilane dendrimers investigated.

Compound	Generation	Surface groups
CRD7	G_0	Sg1
CRD13	G_1	Sg4
CRD27	G_2	Sg8
CRD5	G_0	Sg1
CRD14	G_1	Sg4
CRD28	G_2	Sg8

In the first case (system **A**) one of the dendrimers was firmly bound to siRNA at optimal binding site (estimated free binding energy dG is −57.37 kcal/mol - see Table S1.) and the second one stayed free in solvent in the given simulation. In the second case (system B) we obtained stable dendriplex composed of 16 dedrimers in the form of dimers and trimers bound to siRNA. The rest of dendrimers was divided to one dendrimer dimmer located close to dendriplex and 2 more distant isolated dendrimers.

3.3. Ethidium bromide (EB) intercalation assay

Changes in the fluorescence intensity of the EB-labelled siMcl-1 siRNA in the presence and absence of dendrimers are shown in Fig. 4. Decrease in fluorescence of EB indicates the binding of dendrimers to siRNA with displacement of dye from sites of intercalation. No fluorescence of EB was seen in the presence of naked dendrimers.

The intensity of EB fluorescence gradually decreased with increasing concentration of dendrimers of generation 0 added to the siRNA samples. In the presence of CRDs of generation 1, fluorescence intensity dropped sharply and reached a plateau at a dendrimer/siRNA charge ratio of 2–2.5:1 of **CRD13** and 3:1 of **CRD14**. A similar effect was observed for CRDs of generation 2. Fluorescence intensities reached plateau at the following charge ratios: 1–1.5:1 for **CRD27** and 2:1 for **CRD28**. For dendrimers of generation 0, the quenching response to increased amounts of CRDs was not so effective and fluorescence intensities did not reach stability at dendrimer/siRNA charge ratios of 20:1.

3.4. Gel electrophoresis

Electrophoresis in 3% agarose gel was used to indicate complex formation between siRNA (**siMcl- 1**) and carbosilane ruthenium-terminated dendrimers. Electrophoregrams in Fig. S2 show the mobility rate of naked siRNA (labelled with fluorescein) and dendrimer/siRNA complexes at different charge ratios. Complexes saturated with dendrimers due to their positive surface charge migrate slower than naked siRNA through the gel. CRDs fully retarded the migration of siRNA in the gel at the following charge ratios: 5:1 of dendrimers with imine-pyridine end groups, **CRD13**, **CRD27** and 2.5:1 of dendrimers with pyridine groups **CRD14**, **CRD28**. Dendrimers of generation 0 of both tested groups (**CRD7** and **CRD5**) at the concentration range used were unable to saturate the complex with siRNA (Fig. S2).

Using electrophoresis, we have shown the protective effect of dendrimers on siRNA from degradation by RNase. The line in Fig. 5 shows completely damaged siRNA in the presence of the enzyme. Incubation of siRNA with dendrimers leads to protection of siRNA from RNase, since the addition of heparin before electrophoresis led to siRNA release from the dendriplex and migration through the gel (lanes 3 in Fig. 5). However, not all the CRD dendrimers tested have had a protective effect. **CRD13**, **CRD14** and **CRD28** were able to save the siRNA in the presence of RNase, whereas no protection was seen for **CRD5**, **CRD7** and **CRD27**.

3.5. Zeta potential and hydrodynamic diameter of dendriplexes

To assess the interaction between dendrimers and siRNA and determine the surface charges of the complexes, their zeta potentials were measured. After adding dendrimers to siRNA solution, the initial zeta potential rapidly decreased from −16–20 mV to ~ −40 mV (Fig. 6). Adding dendrimers of generations 1 and 2 led to a sharp increase in zeta potential up to +25.9 ± 1.5 mV -**CRD13**; +26.2 ± 1.3 mV -**CRD27**; +13.3 ± 0.78 mV -**CRD14**; +17.9 ± 0.36 mV -**CRD28**. CRDs of generation 0 (**CRD7** and **CRD5**) had no effect on the zeta potential of formed complexes, maintaining negative values of −40–45 mV over the concentration range tested (Fig. 6A).

The hydrodynamic diameter of the formed complexes was determined by the dynamic light scattering method. After adding

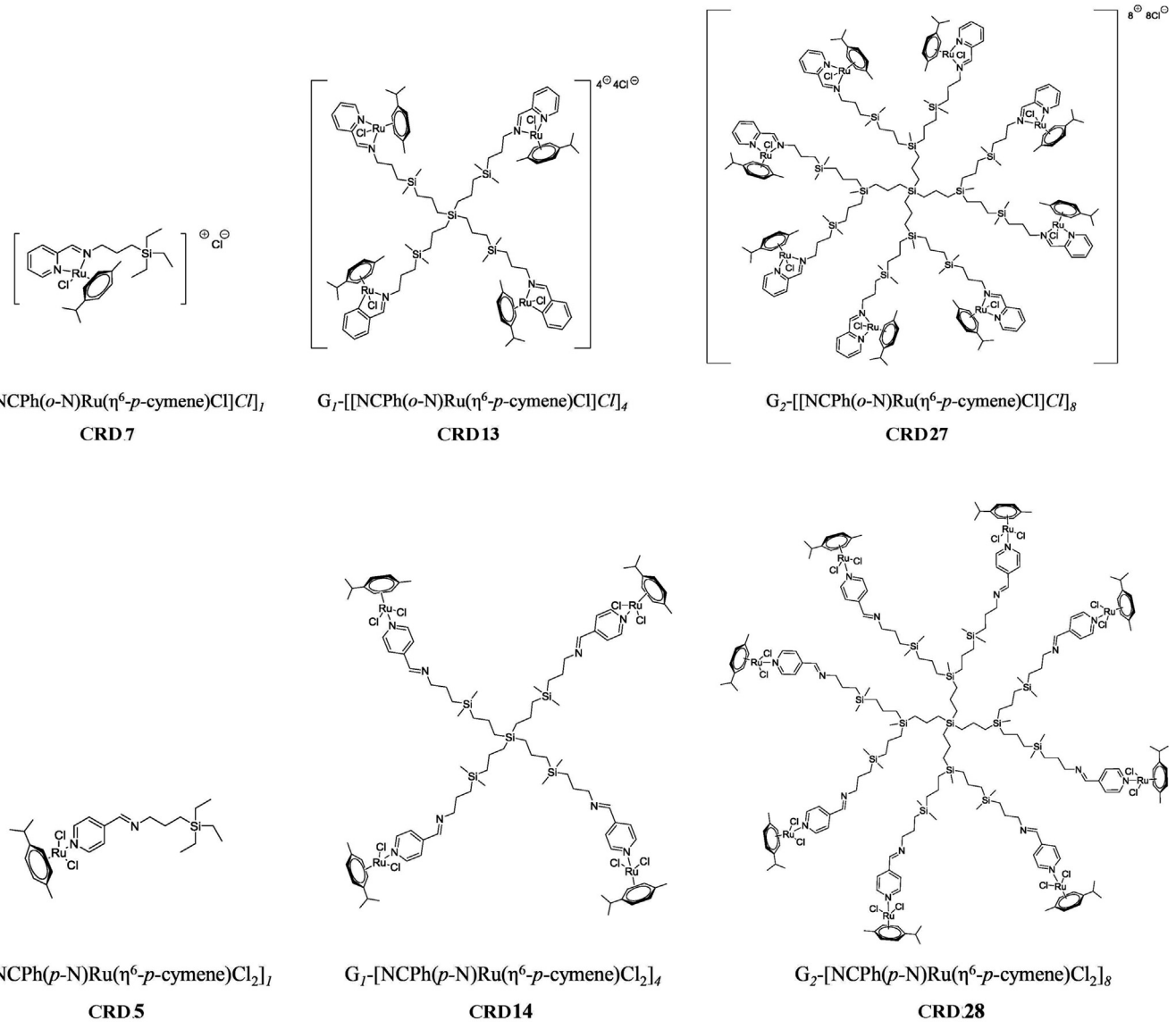

Fig. 1. Molecular structure of ruthenium-terminated carbosilane dendrimers possessing 2 different terminal groups: imine-pyridine: **CRD7**, **CRD13** and **CRD27** (upper panels), and pyridine **CRD5**, **CRD14** and **CRD28** (lower panels).

dendrimers of generation 1 and generation 2 to siRNA suspension, the size of nanoparticles increased up to 1069 ± 185 nm for **CRD13**, 1168.2 ± 92.6 nm for **CRD27**, 1096.9 ± 229.6 nm for **CRD14** and 1032.5 ± 200 nm for **CRD28**. The smallest dendriplexes were formed for complexation of siRNA with CRDs of generation 0 (258.6 ± 89.7) nm in the presence of **CRD5** and 318.5 ± 54.5 nm in the presence of **CRD7** (Fig. 6B).

3.6. Transmission electron microscopy (TEM)

The morphological structure and size of formed dendrimer/siRNA complexes by transmission electron microscopy was first explored in a detailed study of only one siRNA (siBcl-2) as an example. All the dendrimers formed branched complexes with siBcl-2, but the shape of the dendriplexes depended on the generation and type of surface groups of dendrimers. The complexes formed by dendrimers with imine-pyridine end-groups (**CRD7**, **CRD13**, **CRD27**) were more electronically dense than those with pyridine end-groups (**CRD5**, **CRD14**, **CRD28**). The largest structures were formed when siRNA was complexed with **CRD28** (Fig. S3). The size of dendriplexes formed with dendrimers of generation 0 (**CRD5** and **CRD7**) were about 30–800 nm. Similar sizes were found for dendriplexes formed using dendrimers of the 1st generation (**CRD13** and **CRD14**). Most homogenous complexes were seen in the presence **CRD27**. At the base of the microphotographs it was difficult to determine the exact size of complexes due to using drained samples required for this technique. However, these results show that ruthenium-terminated carbosilane dendrimers do form complexes with siRNA.

3.7. Circular dichroism experiments and analysis

CD spectra of free siRNA and siRNA complexed with dendrimers were measured by CD spectroscopy with a Jasco J-815CD spectrometer. Concentrations of CRDs increased over the experiment and ellipticity of siRNA decreased (Fig. 7A, Fig. S4). After adding CRDs to siRNA, the negative peaks (205–215 nm) in the CD spectra completely disappeared. The shape of positive peaks (260–270 nm) was unchanged by dendrimers, but ellipticity values strove to 0 with increasing amounts of dendrimers.

The changes in θ/θ_0 of siRNA CD spectra in the presence of CRDs are shown in Fig. 7B. Adding dendrimers ending with imine-pyridine groups (generation 1 -**CRD13** and generation 2 -**CRD27**) gradually decreased ellipticity values which were close to 0 for the dendrimer/

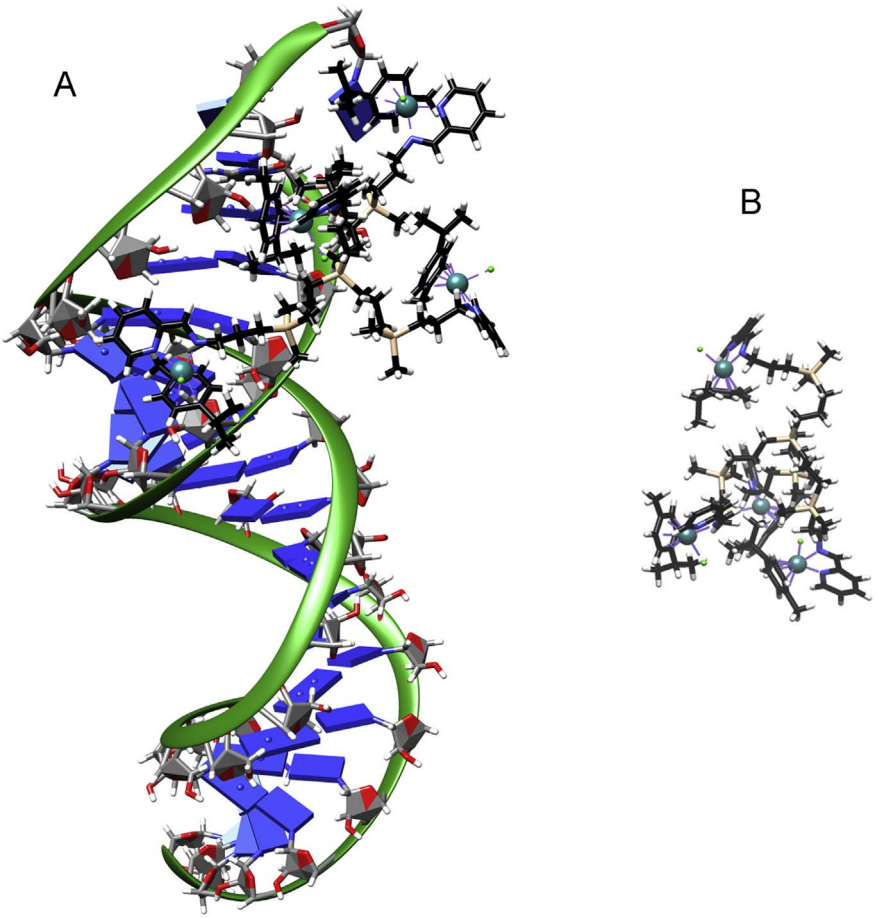

Fig. 2. Simulated system composed of 1 siRNA and 2 CRD13 dendrimers (system A, composed of 2 dendrimers and 1 siRNA). A - dendrimer bound to siRNA at optimal binding site - estimated free binding energy dG is −57.37 kcal/mol. B - the second CRD13 dendrimer which was not complexed with siRNA during the given simulation. Colors: C - gray (siRNA) or black (dendrimer), O - red, H - white, N - blue, Si - beige and the ruthenium atoms are presented as turquoise colored balls. (For interpretation of the references to color in this figure legend, the reader is referred to the web version of this article.)

siRNA charge ratios of 2–2.5:1.

For dendrimers with pyridine end-groups, **CRD14** and **CRD28**, the siRNA complexes were saturated at a dendrimer/siRNA charge ratio near 5:1. The largest number of dendrimer molecules was needed to saturate the complexes of CRD of generation 0 (**CRD5** and **CRD7**), where the dendrimer/siRNA charge ratios were maximal at 5–7:1.

3.8. Cellular uptake

To analyse the ability of ruthenium dendrimers to transfect siRNA cancer cells, flow cytometry and confocal microscopy techniques were used. Dendriplexes internalization into HL-60 cells were examined after 3 h incubation of cells with dendrimer/siRNA complexes. Fig. 8 show that **CRD** dendrimers effectively transfect cells with siRNA.

Dendriplex uptake depended on type and generation. Complexes formed by dendrimers with imine-pyridine groups were taken up more efficiently than those with pyridine groups. Moreover, **CRD** dendrimers of the second generation were more effective compared with dendrimers of the first generation. The most efficient internalization of fluorescein labelled siRNA occurred with complexes formed with **CRD27** (Fig. 8A), where ~30% of cells treated with dendriplexes were loaded by labelled siRNA. Flow cytometry data is closely correlated with that from confocal microscopy technique. The clear green dots seen in HL-60 cells by confocal microscopy indicate the presence of internalized fluorescein labeled siRNA. The most effective transfection was with the **CRD27** dendrimer (Fig. 8A).

4. Discussion

Different types of nanoparticles have been studied as potential carriers of oligonucleotides and siRNA [27–33]. Dendrimers seem to be as excellent non-viral carriers of nucleic acids [34–37]. PAMAM, phosphorus and carbosilane dendrimers form stable dendriplexes with siRNA [4,28], and Dzmitruk et al., (2015) have demonstrated that anti-apoptotic siRNAs complexed with phosphorus dendrimers and delivered to cells can be internalized, inducting apoptosis. However, there are doubts whether interference of anti-apoptotic siRNA alone would be sufficient for the effective treatment of cancer. Due to the fact that ruthenium is a metal with known anti-tumor activity, it therefore seemed appropriate to use ruthenium containing dendrimers as carriers of nucleic acids.

The ability of ruthenium terminated carbosilane dendrimers to form complexes with anti-cancer siRNAs and protect them against nuclease degradation can be seen from our results. To characterize the dendriplexes, zeta-potential and zeta-size were measured for CRDs of 1st and 2nd generation, and was found to increase with the increasing dendrimer/siRNA charge ratio. Positive values of zeta-potential have previously been determined for dendriplexes formed by PAMAM, phosphorus, carbosilane dendrimers and siRNA [4,30,32,38,39]. Similarly, carbosilane dendrimers complexed with oligonucleotides shift zeta potential to positive values [40,31]. Zeta potentials of dendriplexes formed by CRDs of generation 0 (**CRD5** and **CRD7**) were negative due their small number of surface charges. Positively charged dendrimers can interact with biological membranes and aid internalization of the carried molecule. Therefore, in contrast to the dendriplexes formed by CRDs of generation 1st and 2nd, dendrimer/siRNA, complexes containing CRDs of generation 0 may have a lower transfection potential due their negative charge [31]. However, a positive surface charge increases cytotoxicity of the compounds [11]. Zeta size measurements showed that all dendrimers can form complexes with siRNA. The size of the complexes formed by CRDs of generation 0 was < 500 nm, whereas dendriplexes with CRDs of generations 1 and 2 were nearer 1000 nm.

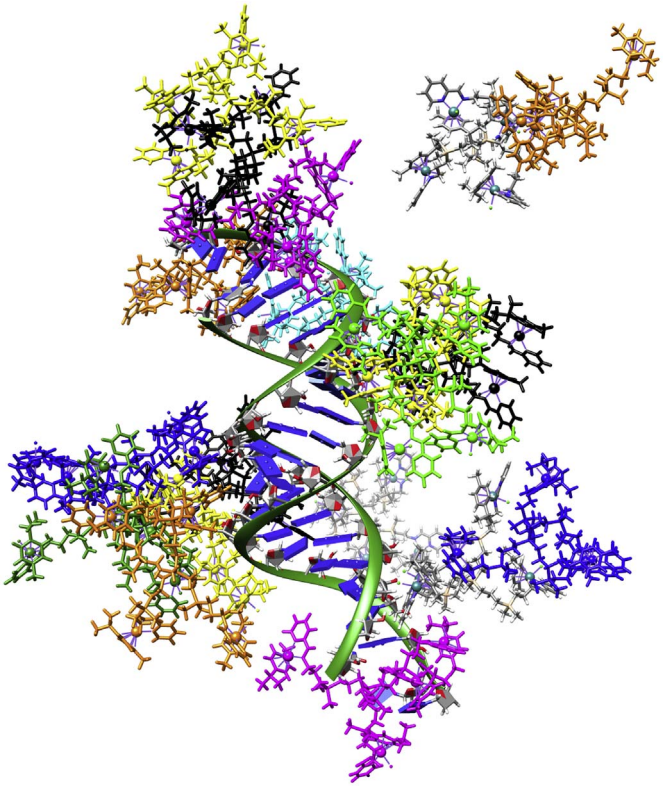

Fig. 3. Simulated system composed of 1 siRNA and 2 CRD13 dendrimers (system **B**, composed of 20 dendrimers and 1 siRNA). Since dendrimers here tend to create clusters, they are differentiated using different colors for better clarity. The ruthenium atoms are presented in ball representation.

Dendriplexes prepared on the basis of siRNA and PAMAM or carbosilane dendrimers were of similar size [4,30,41]. The uptake of such large complexes can be difficult [41], but it has been demonstrated that PAMAM, carbosilane and phosphorus dendrimers can efficiently deliver siRNAs into the cells [5,19,20]. Small particles are taken up by clathrin-dependent endocytosis, whereas particles > 500 nm, such as dendriplexes, are taken up by cells by caveolae [42]. Electron micrograph images indicate the same effect as seen with the zeta method of all our dendrimers complexed with siRNA. Dendriplexes were visible as branched structures that can form aggregate-like inclusions. The largest dendriplexes were seen with **CRD28**. The difference between the TEM and DLS results from dendriplexes is due to the tendency to form aggregates by their strong electrostatic interactions. The samples for the TEM were dried, whereas DLS sizing was measured in solution. Similar discrepancies have been noted described [4,31,43].

The intercalation EB test proved that CRDs of 1st and 2nd generations formed stable complexes with siRNA; their sharply decreased fluorescence intensity. Dendrimers of 2nd generation were more effective in displacing EB from its intercalation sites than those of the 1st generation. EB fluorescence decline was mild in the presence of CRDs of generation 0. Correlation was due to the charge values being proportional to the generation of dendrimers. Thus, the dendrimers with larger numbers of charges can more easily form complexes with siRNA and at lower concentrations [30,41,44,45]. Similar results had been obtained for PAMAM [4], phosphorus [39] and carbosilane dendrimers [4,37].

The molecular dynamics simulations of siRNA/CRD13 systems are showing the ability of dendrimers to create stable complexes with the siRNA. Our estimate of the free energy of binding in the case of 1 dendrimer interacting with siRNA at optimal binding site is −57.37 kcal/mol. Due to the positive charge (+4) of dendrimer and the negative charge of siRNA (−40) there is a strong electrostatic interaction between siRNA and dendrimers in vacuum (EEL contribution) but in water this electrostatic interaction is to a large extent compensated by the polar solvation energetic contribution (EPB) which can be very important for the siRNA release from the complex but also for creation of stable complexes in case of ± charge ratio > 1. So in water the main contributions come from van der Waals (VDW) and non-polar solvation energy contribution (ENP) (for details see Table 1 in Supporting information). Important might be here also the RING-RING (stacking) interactions which are apparent from simulated complexes, i) in case of interactions between the dendrimers and siRNA (see Fig. 1 in Supporting information); ii) between the dendrimers which form small dendrimer clusters (dimers, trimers). As mentioned above, the ability of dendrimers to create dimers/trimers in water can explain the fact of creation of stable siRNA/dendrimer complexes in ± charge ratios higher than 1 and let us emphasize that this is possible just due to the strong screening effect of the polar solvent. This could not be possible in any nonpolar solvent because of strong electrostatic repulsion.

So, we can conclude that molecular modeling confirmed that carbosilane ruthenium dendrimer CRD13 have an advantage to form stable siRNA complexes. This dendrimer is sufficiently flexible which allows its optimal shape adaptation to the surface of the rigid siRNA which increases especially VDW and ENP contributions to the binding energy. Flexibility of these molecules is also important for creation of small dendrimer clusters. In both complexation cases dendrimer/siRNA or

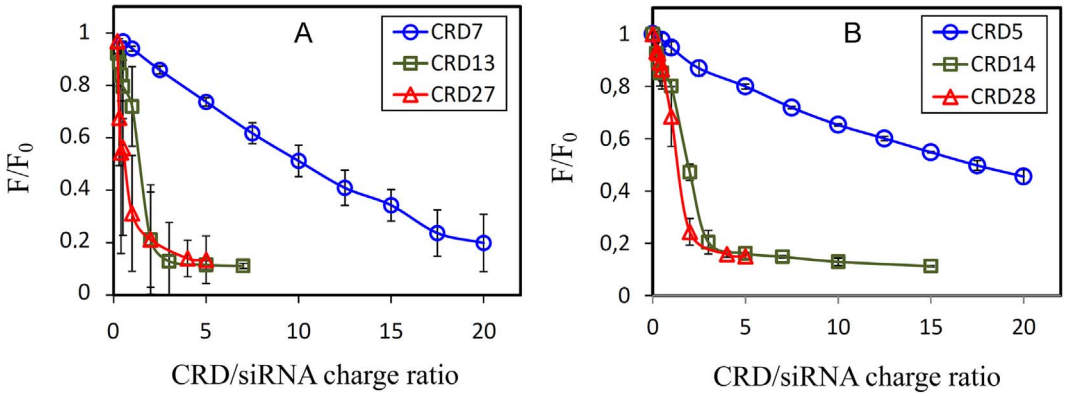

Fig. 4. Changes of EB/siRNA fluorescence intensity after adding CRDs. EB fluorescence intensities are shown as F/F_0, where F is the intensity of fluorescence in the presence of a dendrimers, and F_0 is the intensity in the absence of dendrimers. siRNA (**Mcl-1**) concentration 0.35 μM, EB concentration 0.5 μM in sodium phosphate buffer 10 mM, pH 7.4. $\lambda_{exc.}$ = 480 nm, λ_{em} = 650 nm. Co-ordination of ruthenium: (A) – imine-pyridine groups, **CRD7**, **CRD13**, **CRD27**; (B) - pyridine groups **CRD5**, **CRD14**, **CRD28**. ○ – generation 0; □ – generation 1; Δ – generation 2. Results are mean ± standard deviation (SD), n = 3.

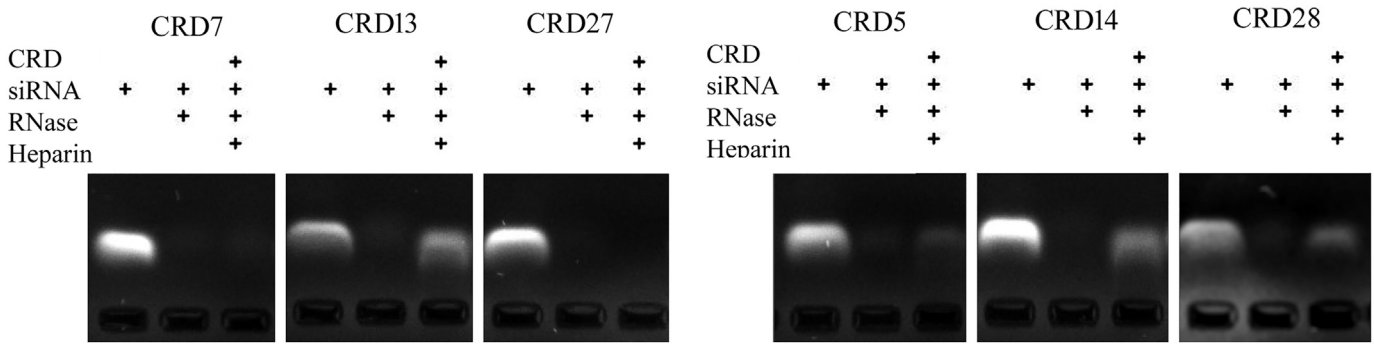

Fig. 5. Protective effect of CRDs on siRNA in the presence of RNase. The first lane demonstrates migration of non-complexed siRNA. The second lane shows migration of siRNA incubated with RNase A (3.0 μg/ml) for 30 min at 37 °C. The third lane gives the migration of siRNA released from the dendriplex in the presence of heparin at 0.082 mg/ml, which shows the protective effect of CRDs on siRNA from damage by RNase.

dendrimer/dendrimer the mutual RING-RING interactions may play important role as well. Especially the fact that CRD13 dendrimer in higher ± charge ratios prefers to create small clusters near the siRNA, which reduces the number of dendrimers interacting sufficiently (optimally) directly with siRNA, it is probably a good promise for creation of rather flexible/porous/soft dendriplexes which might be important for the uptake. Moreover siRNA could be more easily released from such complex inside the cells. Let us note that the last hypothesis about the structure of the real siRNA/CRD13 dendriplexes based on simulation results (the case of siRNA/CRD13 system with ± charge ratio = 2) seems to correlate with TEM results (see TEM microimages in Supporting information).

CD used to determine the effect of dendrimers on the structure of siRNA molecules showed that the presence of dendrimers significantly changes the secondary structure of the siRNAs, which indicates a strong interaction of dendrimers with nucleic acid. These results are in accord with those concerning interactions between carbosilane dendrimers and anti-HIV glicosaminoglicans (GAG1) siRNA [32]. Other studies of interaction between PAMAM or carbosilane dendrimers with siRNA have demonstrated that dendrimers can slightly change the structure of nucleic acid [4,39], which might be related to the type of dendrimer terminal groups. Decline in ellipticity correlated with increasing dendrimer/siRNA charge ratio, indicating the formation of complexes - a similar effect has been described with other dendrimers [4,37,39]. The

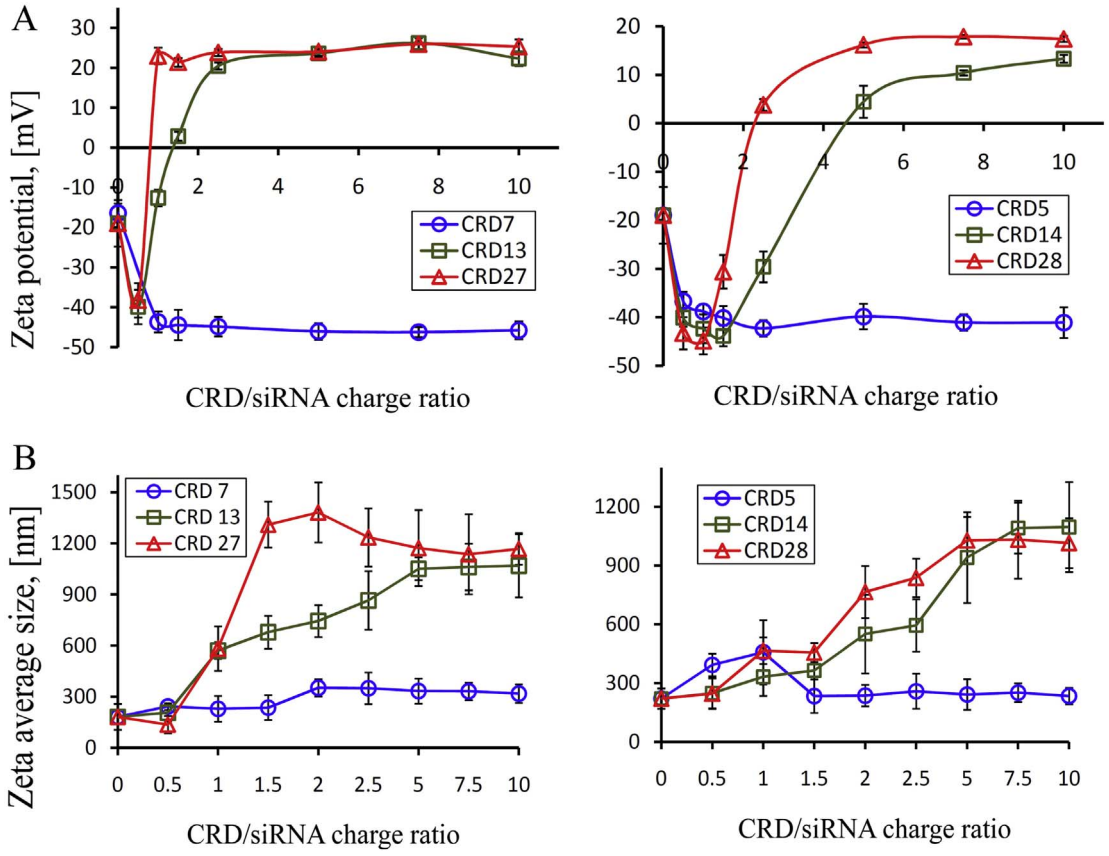

Fig. 6. Zeta potential (A) and Zeta average size (B) of siRNA (**siBcl-2**) with rising concentrations of dendrimers. siRNA concentration 0.3 μM, sodium phosphate buffer 10 mM, pH 7.4. The coordination of ruthenium: (A) – imine-pyridine groups, **CRD7**, **CRD13**, **CRD27**; (B) - pyridine groups **CRD5**, **CRD14**, **CRD28**. ○ – generation 0; □ – generation 1; Δ – generation 2. Results are mean ± standard deviation (SD), n = 3.

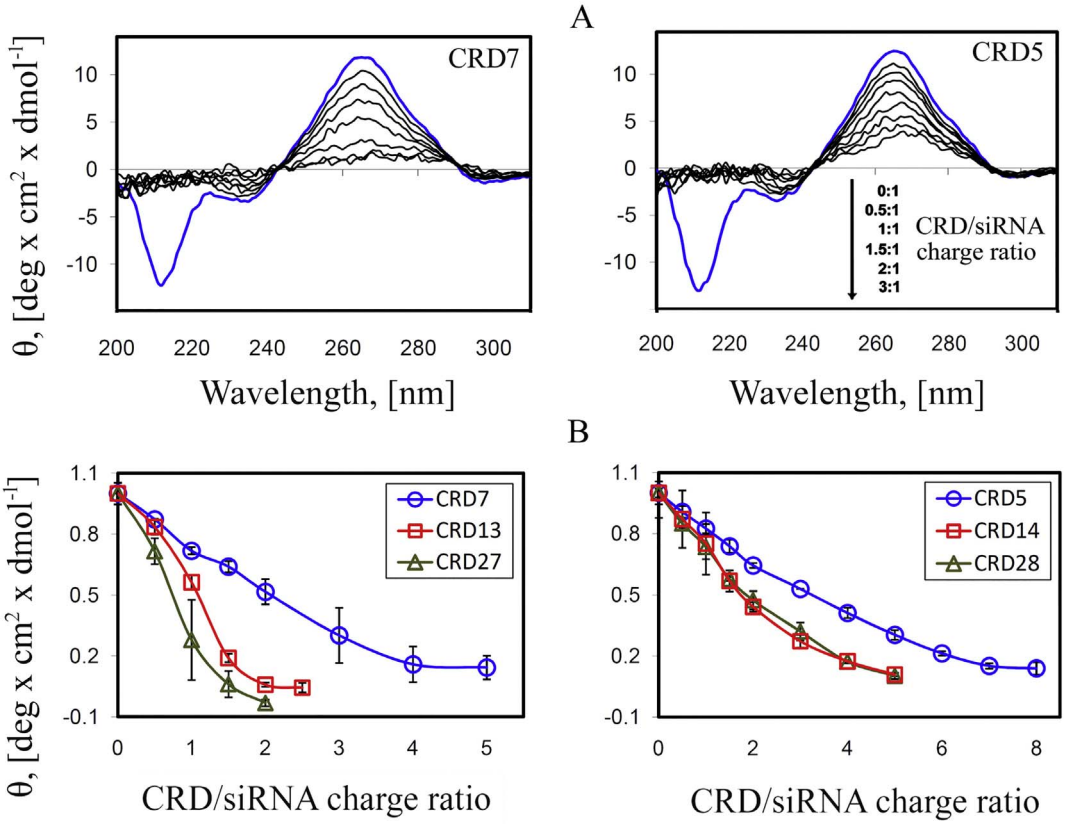

Fig. 7. (A)- CD spectra of siBcl-2 in the presence of: CRD dendrimers ending with imine-pyridine groups (left panels); CRD dendrimers ending with pyridine groups (right panels). (B)- Changes in mean residue ellipticity of **siBcl-2**, at λ = 260 nm in the presence of dendrimers. ○ – generation 0; □ – generation 1; Δ – generation 2. Results are mean ± standard deviation (SD), n = 3. siRNA concentration 2.5 μM, wavelength 200–310 nm, scan speed 50 nm/min, step resolution 0.5 nm, bandwidth 1.0 nm, response time 4 s, Na-phosphate buffer 10 mM, pH 7.4.

siRNAs CD spectra were typical for RNA duplexes A-type, with λ = 210 nm and λ = 260 nm peaks. Reduction of the peaks at the presence of rising concentrations of dendrimers can be explained by the decrease in the absorbance of nucleosides in the complexes formed between siRNA and dendrimers. The CD spectra changes can be result from stacking interactions of base pairs. The results are in agreement with previously published data describing the interactions of dendrimers with RNA [55].

To confirm that CRDs can form complexes with siRNA, electrophoresis was used, as had been carried out previously to register complex formation between oligonucleotides or siRNAs with PAMAM or carbosilane dendrimers [4,38,40,46]. Our siRNA was negatively charged and moved easily through the 3% agarose gel to the cathode. The presence of CRDs in the siRNA solution led to dendrimer/siRNA complexes that had positive surface charge, resulting in their migration in the gel being significantly retarded. With increased amounts of dendrimers the number of free siRNA molecules decreased and retardation was more visible. The data from electrophoresis are closely correlated with those from other techniques we have used. CRD dendrimers, especially those of generations 1 and 2, can form complexes with siRNA. Despite the negative surface charge of our siRNAs, the dendriplexes that formed had pronounced positive charges.

Using electrophoresis, we also demonstrated a protective effect of CRDs against degradation of siRNA by nucleases. Naked siRNA incubated with RNase was completely degraded, whereas dendrimers protected siRNA against degradation; the addition of heparin released the siRNA from the complex, which could then migrate through the gel (Fig. 6). This effect was not visible for dendrimers of generation 0, (**CRD5** and **CRD7**), probably due their weak interaction with molecules of siRNA seen by EB fluorescence (Fig. 4). The lack of any protective effect for **CRD28** has also been reported. Interaction between **CRD28** and siRNA was quite strong, therefore addition of heparin would be insufficient for the release of siRNA from this complex. Thus free siRNA cannot migrate through the gel and no protective effect of this dendrimer was seen. Other dendrimers protected nucleic acid, which was evidenced by naked undigested siRNA being visible on the electrophoregrams. These results are in agreement with those previously obtained for PAMAM and carbosilane dendrimers, but not phosphorus, against nuclease degradation [4,47]. Transfection results presented on the Fig. 8 are correlate with the data obtained previously for the other kinds of dendrimers. PAMAM, phosphorus and carbosilane dendrimers were used for transfection of siRNA to Hela and HL-60 cells [5]. The cell type-dependent uptake and intracellular transport of DNA complexed with polyamidoamine (AuPAMAM) and polyethyleneimine (PEI) dendrimers were described previously [56]. Other studies show that polyethylene glycol (PEG)-conjugated poly-amidoamine (PEG PAMAM) dendrimers were good as non-viral vectors for gene therapy [57].

5. Conclusions

The results show that carbosilane dendrimers associated with anti-cancer siRNAs have the potential to transfect cancer cells with siRNA. Our data also suggest that these dendrimers can protect siRNA against nuclease degradation. Nevertheless, we intend to examine the potential of CRDs in cancer therapy, which might be improved by using classical anti-cancer drugs attached to dendrimer/siRNA complex.

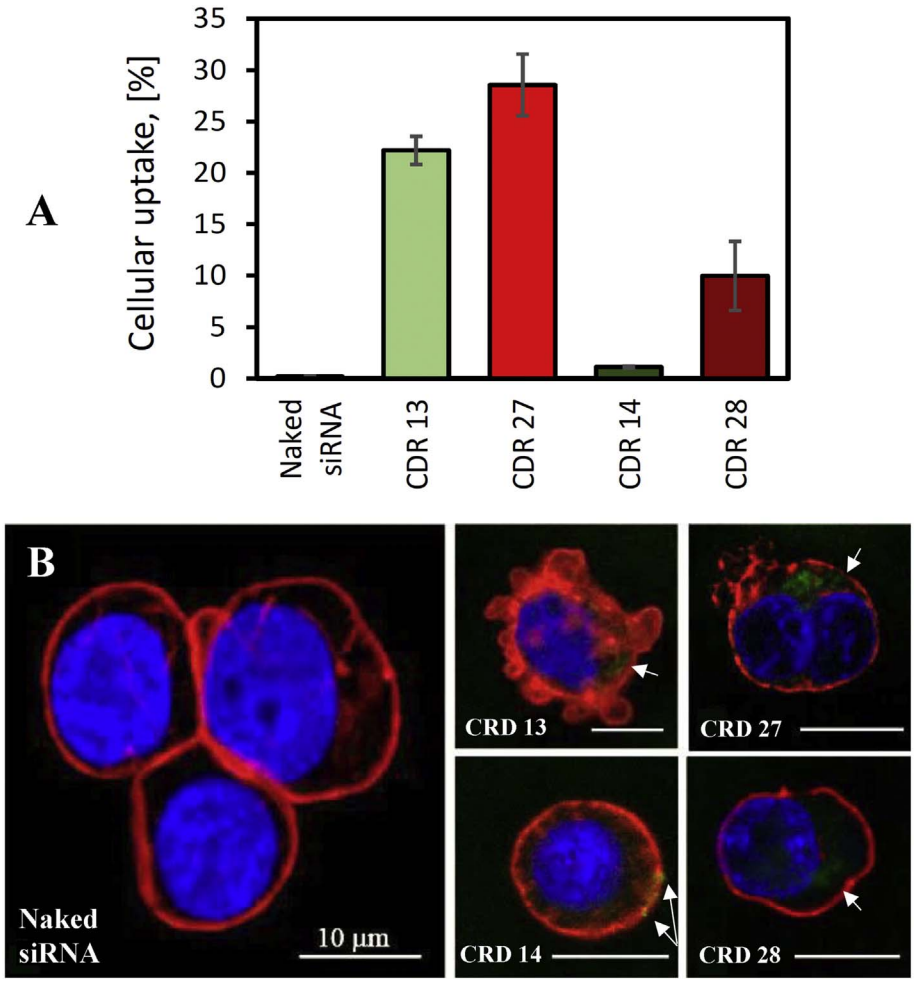

Fig. 8. Flow cytometry (A) of the uptake by HL60 cells of fluorescein labelled siMCL-1 complexed with CRD dendrimers. The results are mean ± standard deviation (SD), n = 3. Confocal microscopy images (B) of HL-60 cells after 3 h incubation with fluorescein labelled siMcL-1 complexed with Ru dendrimers. The concentration of siRNA was 100 nM and the dendrimer/siRNA charge ratio 5:1. Bar = 10 µm.

Abbreviations

Bcl-2	B-cell lymphoma 2 protein
CBS	carbosilane dendrimers
CD	circular dichroism
CRD	carbosilane ruthenium dendrimers
DLS	dynamic light scattering
EB	ethidium bromide
FBS	fetal bovine serum
GAG	glicosaminoglicans
HIV	human immunodeficiency virus
Mcl-xl	myeloid cell leukemia protein
PAMAM	polyamidoamine dendrimers
PBS	phosphate-buffered saline
PEG	polyethylene glycol
PEI	polyethyleneimine
SD	standard deviation
siRNA	small interfering RNA
TAE	Tris-acetate-EDTA buffer
TEM	transmission electron microscopy
UV	ultraviolet
VDW	van der Waals forces

Acknowledgements

This work was co-financed by the Polish Ministry of Science and Higher Education from the research funds for 2013–2016 for realization of international co-financed projects (grant No. W21/7PR/2013), the Marie Curie International Research Staff Exchange Scheme Fellowship within the 7th European Community Framework Programme, project No. PIRSES-GA- 2012-316730 NANOGENE; the Horizon 2020 twinning on DNA-based cancer vaccines project No. H2020-TWINN-2015/CSA-692293 VACTRAIN; the Czech Science Foundation (project No. 15-05903S); the Research Infrastructure NanoEnviCz, supported by the Ministry of Education, Youth and Sports of the Czech Republic under project No. LM2015073.

Appendix A. Supplementary data

Supplementary data to this article can be found online at https://doi.org/10.1016/j.jinorgbio.2018.01.001.

References

[1] N.S. Gandhi, R.K. Tekade, M.B. Chougule, J. Control. Release 194 (2014) 238–256.
[2] R. Tanos, D. Karmali, S. Nalluri, K.C. Goldsmith, BMC Cancer 13 (2016) 16–97.
[3] M. Creixell, N.A. Peppas, Nano Today 7 (4) (2012) 367–379.
[4] M. Ionov, J. Lazniewska, V. Dzmitruk, I. Halets, S. Loznikova, D. Novopashina, E. Apartsin, O. Krasheninina, A. Venyaminova, K. Milowska, O. Nowacka, R. Gomez-Ramirez, F.J. de la Mata, J.P. Majoral, D. Shcharbin, M. Bryszewska, Int. J. Pharm. 485 (2015) 261–269.
[5] V. Dzmitruk, A. Szulc, D. Shcharbin, A. Janaszewska, N. Shcharbina, J. Lazniewska, D. Novopashina, M. Buyanova, M. Ionov, B. Klajnert-Maculewicz, R. Gómez-Ramirez, S. Mignani, J.P. Majoral, M.A. Muñoz-Fernándezg, M. Bryszewska, Int. J. Pharm. 485 (2015) 288–294.
[6] D.S. Conti, D. Brewer, J. Grashik, S. Avasarala, S.R.P. da Rocha, Mol. Pharm. 11 (2014) 1808–1822.
[7] M. Ionov, K. Ciepluch, Z. Garaiova, S. Melikishvili, S. Michlewska, S. Glińska, L. Balcerzak, K. Miłowska, D. Shcharbin, R. Gomez-Ramirez, F.J. de la Mata, I. Waczulikova, M. Bryszewska, T. Hianik, Biochim. Biophys. Acta Biomembr. 1848 (2015) 907–915.
[8] M. Ionov, A. Ihnatsyeu-Kachanb, S. Michlewska, N. Shcharbina, D. Shcharbin,

J.P. Majoral, M. Bryszewska, Int. J. Pharm. 499 (2016) 247–254.
[9] O.M. Merkel, M. Zheng, M.A. Mintzer, G.M. Pavan, D. Librizzi, M. Maly, H. Höffken, A. Danani, E.E. Simanek, T. Kissel, J. Control. Release 153 (2011) 23–33.
[10] M. Ionov, K. Ciepluch, B. Klajnert, S. Glinska, R. Gomez-Ramirez, F.J. de la Mata, M.A. Munoz-Fernandez, M. Bryszewska, Colloids Surf. B: Biointerfaces 101 (2013) 236–242.
[11] J. Wu, W. Huang, Z. He, Sci. World J. (2013) 1–16 630654.
[12] M. Ionov, Z. Garaiova, D. Wróbel, I. Waczulikova, R. Gomez-Ramirez, J. de la Mata, B. Klajnert, M. Bryszewska, T. Hianik, Acta Phys. Univ. Comenia. 1 (2011) 33–39.
[13] S. Biswas, V.P. Torchilin, Pharm. Basel 2 (2013) 161–183.
[14] J. Wang, Z. Lu, M.G. Wientjes, J.L.S. Au, AAPS Journal 12 (2012) 492–503.
[15] M. Hashemi, S.M. Tabatabai, H. Parhiz, S. Milanizadeh, S.A. Farzad, K. Abnous, M. Ramezani, Mater. Sci. Eng. C61 (2016) 791–800.
[16] Y.M. Arteta, M.L. Ainalem, L. Porcar, A. Martel, H. Coker, D. Lundberg, D.P. Chang, O. Soltwedel, R. Barker, T. Nylander, J. Phys. Chem. B 118 (2014) 12892–12906.
[17] L.B. Jensen, G.M. Pavan, M.R. Kasimova, S. Rutherford, A. Danani, H.M. Nielsen, C. Foged, Int. J. Pharm. 416 (2011) 410–418.
[18] N. De Las Cuevas, S. Garcia-Gallego, B. Rasines, F.J. de la Mata, L.G. Guijarro, M.A. Muñoz-Fernández, R. Gomez, Curr. Med. Chem. 19 (2012) 5052–5061.
[19] L. Palmerston Mendes, J. Pan, P. Torchilin, Molecules 22 (2017) 1401–1423.
[20] V. Leiro, S.D. Santos, A.P. Pego, Delivering siRNA with dendrimers: in vivo applications, Curr. Gene. Ther. 17 (2) (2017) 105–119.
[21] S. Michlewska, M. Ionov, D. Shcharbin, M. Maroto-Díaz, R. Gomez Ramirez, F.J. de la Mata, M. Bryszewska, Eur. Polym. J. 87 (2017) 39–47.
[22] I. Dragutan, V. Dragutan, A. Demonceau, Molecules 20 (2015) 17244–17274.
[23] R. Carter, A. Westhorpe, M.J. Romero, A. Habtemariam, C.R. Gallevo, Y. Bark, N. Menezes, P.J. Sadler, R.A. Sharma, Sci. Report. 6 (20596) (2016) 1–12.
[24] S. Spreckelmeyer, C. Orvig, A. Casini, Molecules 19 (2014) 15584–15610.
[25] M. Maroto-Díaz, B.T. Elie, P. Gómez-Sal, J. Pérez-Serrano, R. Gómez, M. Contel, F.J. de la Mata, Dalton Trans. 45 (2016) 7049–7066.
[26] J. Olmsted, D.R. Kearns, Biochemist 16 (1977) 3647–3654.
[27] M.J. Serramía, S. Álvarez, E. Fuentes-Paniagua, M.I. Clemente, J. Sánchez-Nieves, R. Gómez, J.F. de la Mata, M.A. Muñoz-Fernández, J. Control. Release 200 (2014) 60–70.
[28] D. Wrobel, K. Kolanowska, A. Gajek, R. Gomez-Ramirez, J.P. de la Mata, E. Pedziwiatr-Werbicka, B. Klajnert, I. Waczulikova, M. Bryszewska, Biochim. Biophys. Acta Biomembr. 1838 (2014) 882–889.
[29] J. Sánchez-Nieves, P. Fransen, D. Pulido, R. Lorente, M.A. Muñoz-Fernández, F. Albericio, M. Royo, R. Gómez, J.F. de la Mata, Eur. J. Med. Chem. 76 (2014) 43–52.
[30] M. Ionov, Z. Garaiova, I. Waczulikova, D. Wróbel, E. Pędziwiatr-Werbicka, R. Gomez-Ramirez, F.J. de la Mata, B. Klajnert, T. Hianik, M. Bryszewska, Biochim. Biophys. Acta Biomembr. 1818 (9) (2012) 2209–2216.
[31] E. Pedziwiatr-Werbicka, D. Shcharbin, J. Maly, M. Maly, M. Zaborski, B. Gabara, P. Ortega, J.F. de la Mata, R. Gómez, M.A. Muñoz-Fernandez, B. Klajnert, M. Bryszewska, J. Biomed. Nanotechnol. 8 (1) (2012) 57–73.
[32] D. Shcharbin, E. Pedziwiatr, O. Nowacka, M. Kumarb, M. Zaborsk, P. Ortega, F.J. de la Mata, R. Gómez, M.A. Muñoz-Fernandeze, M. Bryszewska, Colloids Surf. B: Biointerfaces 83 (2011) 388–391.
[33] N. Weber, P. Ortega, M.I. Clemente, D. Shcharbin, M. Bryszewska, J.F. de la Mata, R. Gómez, M.A. Muñoz-Fernandeze, J. Control. Release 132 (15) (2008) 5–64.
[34] A. Dehshahri, H. Sadeghpour, Colloids Surf. B: Biointerfaces 132 (2015) 85–102.
[35] C.Y. Li, H.J. Wang, J.M. Cao, J. Zhang, X.Q. Yu, Eur. J. Med. Chem. 87 (2014) 413–420.
[36] K. Ciepluch, M. Ionov, J.P. Majoral, M.A. Muñoz-Fernández, M. Bryszewska, J. Lumin. 148 (2014) 364–369.
[37] E. Pedziwiatr-Werbicka, E. Fuentes, V. Dzmitruk, J. Sánchez-Nieves, M. Sudas, E. Drozd, A. Shakhbazau, D. Shcharbin, F.J. de la Mata, R. Gomez-Ramirez, M.A. Muñoz-Fernandez, M. Bryszewska, Colloids Surf. B: Biointerfaces 109 (2013) 183–189.
[38] J.P. Nam, K. Nam, S. Jung, J.W. Nah, S.W. Kim, J. Control. Release 209 (2015) 179–185.
[39] M. Ferenc, E. Pedziwiatr-Werbicka, K.E. Nowak, B. Klajnert, J.P. Majoral, M. Bryszewska, Molecules 18 (4) (2013) 4451–4466.
[40] L.T. Thuy, S. Mallick, J.S. Choi, Int. J. Pharm. 492 (2015) 233–243.
[41] C. Chen, P. Posocco, X. Liu, Q. Cheng, E. Laurini, J. Zhou, C. Liu, Y. Wang, J. Tang, V.D. Col, T. Yu, S. Giorgio, M. Fermeglia, F. Qu, Z. Liang, J.J. Rossi, M. Liu, P. Rocchi, S. Pricl, L. Peng, Small 12 (27) (2016) 3667–3676.
[42] B. Nichols, J. Cell Sci. 116 (2003) 4707–4714.
[43] M. Ionov, K. Ciepluch, B.R. Moreno, D. Appelhans, J. Sánchez-Nieves, R. Gómez, F.J. de la Mata, M.A. Muñoz-Fernández, M. Bryszewska, Cur, Med. Chem. 20 (2013) 3935–3943.
[44] A. Shakhbazau, I. Isayenka, N. Kartel, N. Goncharova, I. Seviaryn, S. Kosmacheva, M. Potapnev, D. Shcharbin, M. Bryszewska, Int. J. Pharm. 383 (2010) 228–235.
[45] H. Suzuki, M. Mori, M. Suzuki, K. Sakurai, S. Miura, H. Ishii, Cancer Lett. 115 (2) (1977) 243–248.
[46] M. Ionov, D. Wróbel, K. Gardikis, S. Hatziantoniou, C. Demetzos, J.P. Majoral, B. Klajnert, M. Bryszewska, Chem. Phys. Lipids 165 (2012) 408–413.
[47] G.M. Pavan, A. Danani, J. Drug Deliv, Sci. Technol. 22 (2012) 83–89.
[48] J.M. Wang, R.M. Wolf, J.W. Caldwell, P.A. Kollman, D.A. Case, J. Comput. Chem. 25 (2004) 1157–1174.
[49] C.I. Bayly, P. Cieplak, W.D. Cornell, P.A. Kollman, J. Phys. Chem. 97 (1993) 10269–10280.
[50] F. Dupradeau, A. Pigache, T. Zaffran, C. Savineau, R. Lelong, N. Grivel, D. Lelong, W. Rosanski, P. Cieplak, Phys. Chem. Chem. Phys. 12 (2010) 7821–7839.
[51] M.S. Gordon, M.W. Schmidt, The First Forty Years, Elsevier, Amsterdam, 2005, pp. 1167–1189.
[52] R. Salomon-Ferrer, A.W. Goetz, D. Poole, S.L. Grand, R.C. Walker, J. Chem. Theory Comput. 9 (2013) 3878–3888.
[53] D.A. Case, D.S. Cerutti, T.E. Cheatham III, T.A. Darden, R.E. Duke, T.J. Giese, H. Gohlke, A.W. Goetz, D. Greene, N. Homeyer, S. Izadi, A. Kovalenko, T.S. Lee, S. LeGrand, P. Li, C. Lin, J. Liu, T. Luchko, R. Luo, D. Mermelstein, K.M. Merz, G. Monard, H. Nguyen, I. Omelyan, A. Onufriev, F. Pan, R. Qi, D.R. Roe, A. Roitberg, C. Sagui, C.L. Simmerling, W.M. Botello-Smith, J. Swails, R.C. Walker, J. Wang, R.M. Wolf, X. Wu, L. Xiao, D.M. York, P.A. Kollman, AMBER 2017, University of California, San Francisco, 2017.
[54] E.F. Pettersen, T.D. Goddard, C.C. Huang, G.S. Couch, D.M. Greenblatt, E.C. Meng, T.E. Ferrin, J. Comput. Chem. 25 (2004) 1605–1612.
[55] J. Reyes-Reveles, R. Sedaghat-Herati, D.R. Gilley, A.M. Schaeffer, K.C. Ghosh, T.D. Greene, H.E. Gann, W.A. Dowler, S. Kramer, J.M. Dean, R.K. Delong, Biomacromolecules 14 (2013) 4108–4115.
[56] E. Figueroa, P. Bugga, V. Asthana, A.L. Chen, J.S. Yan, E.R. Evans, R.A. Drezek, J. Nanobiotechnol. 15 (2017) 36.
[57] L. Xu, W. Shen, B. Wang, X. Wang, G. Liu, Y. Tao, R. Qi, Curr. Drug Deliv. 13 (2016) 590–599.